Appl Phys B (2010) 100: 109–115
DOI 10.1007/s00340-010-4063-1

Applied Physics B
Lasers and Optics

Light absorption in undoped congruent and magnesium-doped lithium niobate crystals in the visible wavelength range

J.R. Schwesyg · M.C.C. Kajiyama · M. Falk · D.H. Jundt · K. Buse · M.M. Fejer

Received: 20 April 2010 / Published online: 29 May 2010

Abstract Light absorption measurements of nominally undoped congruent lithium niobate crystals (CLN) as well as 5 mol% magnesium-oxide-doped lithium niobate (MgO:LN) crystals were performed in the light wavelength range of 350 to 800 nm. Absorption spectra reveal that—besides iron (Fe) impurities—chromium (Cr) impurities of less than 0.5 wt. ppm concentration contribute significantly to the total optical absorption in the CLN crystals with a maximum of 0.035 cm^{-1} around 500 nm. The axial distribution of Cr within a CLN boule is examined, revealing that the bottom part of the boule contains less Cr and therefore light absorption is reduced as well. In the case of the MgO:LN crystals, Cr impurities also contribute significantly to the total optical absorption, which is on the order of 0.025 cm^{-1} for ordinarily polarized light and 0.015 cm^{-1} for extraordinarily polarized light around 500 nm.

1 Introduction

Due to its large nonlinear-optical coefficients and its commercial availability, lithium niobate ($LiNbO_3$) is an important material for nonlinear-optical applications, e.g. second-harmonic generation (SHG) or optical parametric oscillation (OPO). Obstacles such as the photorefractive effect are overcome by various techniques, of which the most common is doping with 5 mol% magnesium oxide (MgO) [1] or operating undoped congruent $LiNbO_3$ (CLN) crystals at elevated temperatures of about 200°C [2]. However, for applications in the multi-watt-average-power regime, optical absorption can also be a serious obstacle. Although the optical quality of the commercially available crystals is very good and the absorption levels are small, these small absorption losses limit the usability of $LiNbO_3$ crystals, e.g. optical absorption increases OPO pump power thresholds and absorption-induced heating can disturb the phase matching in nonlinear optical setups, cause thermal lensing, or even destroy the $LiNbO_3$ crystal. An estimate of the effects of thermal loading at 480 nm is given in the following: with a power of 5 W, a typical beam radius of 100 µm, and an absorption coefficient of $\alpha = 0.01\ cm^{-1}$, which is below the detection threshold for measurements using 1 mm thick CLN or MgO:LN crystals, one can estimate the induced maximum temperature change within the beam area to be about 0.2°C [3]. With the thermo-optic coefficient for extraordinarily polarized light of $5 \times 10^{-5}°C^{-1}$ [4], this temperature rise leads to a refractive-index change of about 1×10^{-5}. Such a refractive-index change seriously affects phase matching and furthermore leads to thermal lensing with an effective focal length of less than 1 cm.

So far, most studies of absorption in $LiNbO_3$ have focused on multi-valence transition-metal impurities such as iron (Fe), copper (Cu), or manganese (Mn), because these impurities can be present in different valence states enabling charge-transfer transitions and thus can cause absorption and photorefractive damage in lithium niobate crystals [5]. Now, since photorefraction can be suppressed, the dominating question is whether other impurities that are mainly incorporated in a single valence state, e.g. such as chromium

J.R. Schwesyg (✉) · M.M. Fejer
E. L. Ginzton Laboratory, Stanford University, Stanford, CA 94305, USA
e-mail: schwesyg@physik.uni-bonn.de

J.R. Schwesyg · K. Buse
Institute of Physics, University of Bonn, Wegelerstr. 8, 53115, Bonn, Germany

M.C.C. Kajiyama · M. Falk · D.H. Jundt
Crystal Technology, Inc., 1040 East Meadow Circle, Palo Alto, CA 94303, USA

(Cr^{3+}) or nickel (Ni^{2+}) ions, contribute significantly to light absorption in the crystals as well.

In this paper, we report on small absorption peaks of CLN and 5 mol% MgO-doped $LiNbO_3$ (MgO:LN) crystals in the wavelength range from 350 to 800 nm. First, the main impurities causing the optical absorption are identified by comparing the characteristic absorption peaks to absorption data from lithium niobate crystals that are intentionally doped with transition-metal ions. It turns out that the most characteristic absorption peaks are caused by Cr impurities. Then, the segregation of Cr within CLN and light polarization dependences of the absorption spectra in CLN and MgO:LN are studied.

2 Experimental setup

Commercial vendors of lithium niobate crystals typically control impurity levels of transition metals to values lower than 1 wt. ppm. Therefore, a rather large optical path length on the order of 20 mm or more is required in order to easily detect absorption bands caused by unintentionally incorporated impurities by conventional spectrophotometric means.

Several $LiNbO_3$ samples, undoped and MgO-doped, provided by Crystal Technology, Inc., were investigated. On the one hand, congruent $LiNbO_3$ crystals can be grown efficiently, with large fractions from the initial melt charge being converted into crystalline material, having no or minimal axial composition variations. On the other hand, due to a distribution coefficient for Mg that is larger than unity, MgO-doped $LiNbO_3$ crystals present measurable axial composition variations [6], in effect restricting how much crystalline material can be pulled from an initial melt charge. Thus, two CLN crystal cubes, of dimensions $20 \times 20 \times 20$ mm^3, were cut from a grown boule of which the fraction of melt converted to crystal material exceeded 80%. This high conversion factor is commonly used for CLN SAW (surface acoustic wave)-grade crystal growth, and helps to reveal segregation of impurities that lead to concentration gradients along the growth axis. The two cubes are cut from this specially grown boule, using the same raw materials as used for the growth of optical-quality CLN boules, and they were oriented following standard convention orientation for the x, y, and z principal axes with respect to the crystal boule. The solidified fraction, defined as the crystallized portion of material over the initial melt charge, was approximately 15% for the CLN cube fabricated from the top part of the boule, whereas the sample fabricated from the bottom part of the boule corresponded to a solidified fraction of about 70%. The x-faces were polished to high optical quality. Four MgO:LN samples with the dimensions $25 \times 15 \times 20$ mm^3 from one MgO:LN boule were examined. The x-faces were polished, resulting in an optical path length along the x-axis of 25 mm. All MgO:LN samples were cut from the same slab from the center of the boule. For comparison, a 1-mm-thick z-plate from the top part of a Cr_2O_3-doped $LiNbO_3$ boule doped with 102 wt. ppm Cr in the melt was also studied. Two samples, one each from the top and bottom of the CLN boule, were used for impurity analysis. The impurity levels were measured by glow discharge mass spectrometry (GDMS) at Shiva Technologies (Evans Analytical Group).

High-precision light transmission measurements were performed with a Varian Cary 500 absorption spectrophotometer. A Glan–Taylor polarizing prism was used as polarizer. In order to maintain stable conditions, the measurement chamber was purged with dried air. The obtained absorption spectra were corrected for Fresnel reflection losses [7] by using Sellmeier equations available in the literature for CLN and MgO:LN [8]. In order to determine the peak positions, one ideally would subtract the intrinsic band edge absorption. Unfortunately, absorption measurements in the blue and UV spectral ranges are very sensitive to light scattering, which increases steeply with decreasing wavelength and which adds additional loss. An imperfect Fresnel correction adds further uncertainty. Therefore, in order to determine the correct shape and magnitude of the absorption peaks, a common procedure in spectroscopy is used, which assumes that the background can be approximated by a straight line in the vicinity of an absorption peak [9]. Hence, Gaussian line shapes on top of a straight line are fitted to the observed absorption peaks within the respective spectral ranges. In the following the peak width $2w$ ($\frac{1}{e^2}$ value) relates to the full width at half-maximum ($FWHM$) according to $FWHM = 2w\sqrt{2\ln 2}$.

3 Results and analysis

3.1 Undoped congruent lithium niobate

Absorption spectra of CLN from the top part of the boule (solid line) and the bottom part (dashed line) are shown in Fig. 1 for ordinarily polarized light (o-wave) (a) and for extraordinarily polarized light (e-wave) (b). Absorption features covering significant parts of the visible spectrum are clearly seen. The peak positions and width parameters w are summarized in Table 1. Although the peak fits show less than 1% error, the fits slightly depend on the definition of the peak boundaries. Hence, different choices of peak boundaries lead to slightly different results in fitting. Therefore, every fit is performed about five times with slightly different peak boundaries in order to get a set of averaged values for the peak position, width, and amplitude. The errors of the peak positions and the peak amplitudes are about 1% for the top CLN cube and about 2% for the bottom CLN cube, and the errors of w are about 5% for the top-cube spectra and 20% for the bottom-cube spectra. It is important to

Table 1 Spectral positions of the absorption bands of the CLN crystals for ordinarily and extraordinarily polarized light. Entries marked with N/A indicate that fitting was not possible. In this case, the position of the absorption peak is assumed to be the same as the position of the local maximum absorption

Crystal	Peak (cm^{-1})	w (cm^{-1})	Fit amplitude (cm^{-1})
CLN top: o-wave	13 750	70	0.0023
	15 300	900	0.0174
	20 850	400	0.0023
	23 400	400	0.0006
CLN bottom: o-wave	13 750	N/A	N/A
	15 500	600	0.0023
	20 900	N/A	N/A
	23 400	N/A	N/A
CLN top: e-wave	13 650	200	0.0006
	15 550	1500	0.0065
	21 350	700	0.0040
CLN bottom: e-wave	15 650	300	0.0010
	21 300	600	0.0018

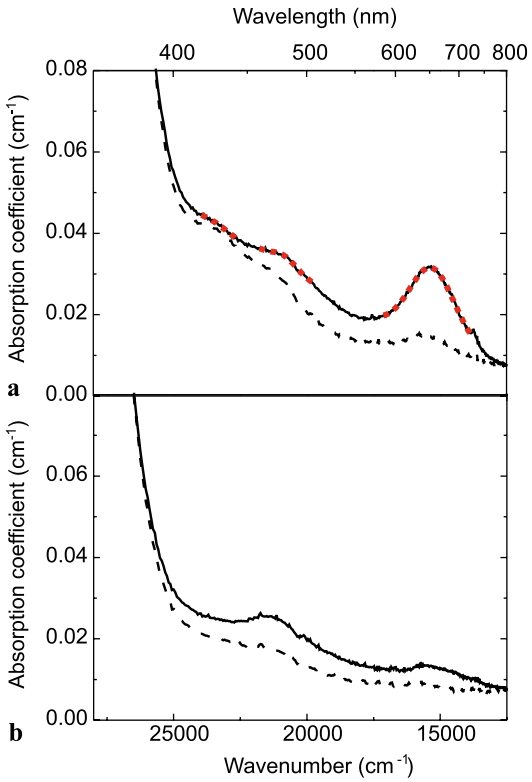

Fig. 1 Absorption coefficient versus wavenumber for ordinarily polarized light **a** and extraordinarily polarized light **b** in CLN from the top part of the boule (*solid line*) and the bottom part of the boule (*dashed line*). Gaussian peak fits with baseline correction are performed for all spectra in order to determine peak positions, widths, and amplitudes. As an example, the fits for the top part of the o-wave spectrum are presented (*red square-dotted line*)

Table 2 GDMS results for CLN

Wt. ppm	Fe	Cr	Ni	Cu
Top	1.20	0.50	0.14	0.09
Bottom	1.10	0.06	< 0.01	< 0.05

note that, in the case of a small broad absorption peak on top of a larger absorption shoulder, errors from assuming a linear peak background will appear, although the respective peak fit might have a very small error and results are averaged over several fitting procedures. This is the case, for example, for the e-wave spectrum of the bottom CLN cube. However, the narrow peaks at 13 750 cm^{-1} (o-wave) and 13 650 cm^{-1} (e-wave) can be determined to an accuracy of 0.3%.

For both o-wave and e-wave light, the absorption in the bottom part of the boule is drastically decreased over the entire spectrum. In the bottom part, the absorption peak at 15 500 cm^{-1} almost vanishes.

The GDMS results show that mainly four transition-metal impurities are incorporated. The results are summarized in Table 2. We note that while the GDMS technique can resolve trace impurities down to sub-parts per million and even parts per billion when interferences are not present, the precision (reproducibility) of the technique is about 30%. The Cr concentration changes dramatically from top to bottom. For Cu and Ni this is also the case, but the concentrations of Cu and Ni in the top part of the boule are already much lower than the concentration of Cr in the top part. The only impurity that is evenly distributed within the crystal is Fe.

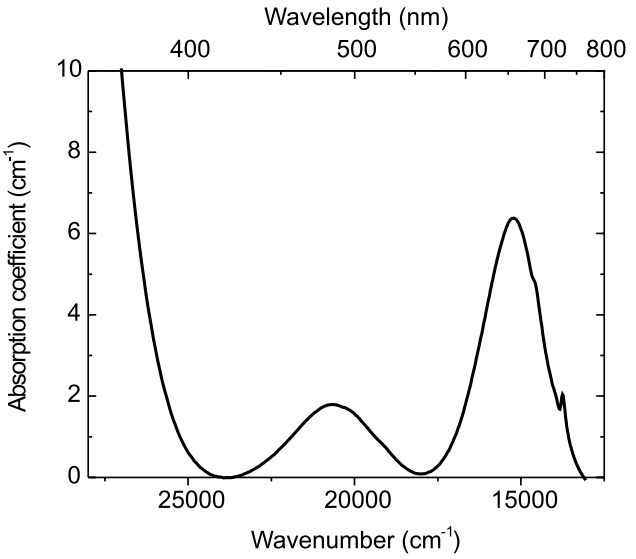

Fig. 2 Absorption coefficient for ordinarily polarized light versus wavenumber for intentionally Cr_2O_3-doped $LiNbO_3$ (102 wt. ppm Cr in the melt, top part of the boule)

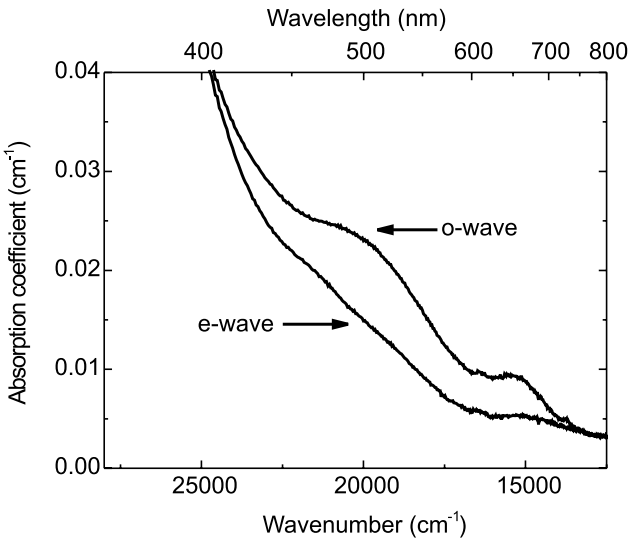

Fig. 3 Absorption coefficient for ordinarily and extraordinarily polarized light versus wavenumber for 5 mol% MgO-doped $LiNbO_3$

The measured absorption spectrum for the 1 mm thick slice of the intentionally Cr-doped crystal for ordinary light polarization is shown in Fig. 2.

3.2 Magnesium-doped lithium niobate

There is no significant difference between absorption spectra from various MgO:LN crystals cut from the same slab, within the accuracy of the measurement, indicating that the absorbing species is uniformly distributed in the plane normal to the growth direction. Representative absorption spectra of one of the MgO:LN crystals are shown in Fig. 3 for both polarizations. Here, fewer absorption peaks can be determined than for the CLN crystals, as can be seen in Table 3.

Table 3 Spectral positions of the absorption bands of the MgO:LN crystals for ordinarily and extraordinarily polarized light

Crystal	Peak (cm^{-1})	w (cm^{-1})	Fit amplitude (cm^{-1})
MgO:LN: o-wave	13 750	100	0.0006
	15 200	660	0.0029
	19 000	750	0.0022
	20 350	760	0.0023
MgO:LN: e-wave	15 050	1000	0.0012
	18 800	650	0.0002
	21 300	480	< 0.0001

The errors of the peak positions and the peak amplitudes are about 1% for the o-wave and about 2% for the e-wave light, and the errors of w are about 5% for o-wave and 20% for e-wave light. As in the case of CLN, the narrow peak at 13 750 cm^{-1} (o-wave) is determined with an accuracy of 0.3%. For e-wave light, no peak can be determined around 13 750 cm^{-1}. Furthermore, the same error considerations and error sources as for CLN have to be taken into account.

4 Discussion

4.1 Impurities in congruent lithium niobate

The absorption spectra were analyzed by comparison with literature absorption data for intentionally doped lithium niobate crystals. A summary of the most common impurities and their absorption peaks is listed in Table 4.

4.1.1 Chromium

The o-wave spectra of undoped $LiNbO_3$ crystals from the top and bottom parts of the boule in Fig. 1a show absorption peaks centered at the same spectral positions as in the o-wave spectrum of the Cr_2O_3-doped $LiNbO_3$ crystal in Fig. 2. For o-wave spectra, the most pronounced absorption peaks are centered at 15 300 and 20 850 cm^{-1}. In the case of e-wave light, the absorption peak at 21 350 cm^{-1} in Fig. 1b is consistent with Cr^{3+} absorption peaks known from the literature (see Table 4) as well. The smaller e-wave absorption around 15 550 cm^{-1} also agrees with the Cr^{3+} absorption literature value within the accuracy of the measurement and is also present in both the top and bottom CLN samples. Additionally, for the o-wave light in CLN shown in Fig. 1a as well as in the Cr_2O_3-doped $LiNbO_3$ spectrum in Fig. 2, the characteristic narrow absorption peak around 13 750 cm^{-1} is present for the o-wave light (Table 4). For e-wave illumination the characteristic peak appears around 13 650 cm^{-1},

Table 4 Spectral positions of known absorption bands of intentionally doped $LiNbO_3$ crystals for ordinarily and extraordinarily polarized light

Ion	o-wave		e-wave		References
	Peak (cm^{-1})	Peak (nm)	Peak (cm^{-1})	Peak (nm)	
Cr^{3+}	13 820	724	13 780	725	[10]
	15 330	652	15 300	653	
	20 850	480	21 390	468	
Fe^{2+}	20 970	477	21 510	465	[11, 12]
Fe^{3+}	20 570	486	N/A	N/A	[11, 12]
Ni^{2+}	13 330	750	13 900	719	[13]
	20 410	490	19 420	515	
	23 360	428	21 980	455	
Cu^{+}	26 670	375			[11, 14]

which agrees with literature data as well (Table 4). Comparison of the peaks in Table 1 to literature values from Table 4 shows that, of the four impurities determined with GDMS measurements (Table 2), only Cr^{3+} can absorb in all three spectral regions, around 13 850, 15 300, and 21 000 cm^{-1} for o-wave and e-wave light. Thus, we assume that Cr^{3+} impurities cause the dominant absorption features in the CLN samples.

4.1.2 Iron

It is interesting to note that the o-wave absorption peak around 15 300 cm^{-1} in the bottom part of the boule almost vanishes, whereas this is not fully the case in the region around 20 850 cm^{-1}; a shoulder remains. The most probable impurity to cause this absorption shoulder is Fe^{2+}. According to the GDMS data in Table 2, the Fe content is almost the same for top and bottom, predicting an o-wave absorption peak centered around 20 970 cm^{-1} and extending from 16 000 to 24 000 cm^{-1} [11]. Hence, the Fe content probably contributes significantly to the remaining absorption shoulder around 20 850 cm^{-1}. Unfortunately, the actual Fe^{2+} content is unknown. With the known Fe^{2+} o-wave-absorption cross section at 20 970 cm^{-1}, $\sigma_{Fe^{2+}} = 4.63 \times 10^{-18}$ cm^2 [11], and assuming that the maximum contribution from Fe^{2+} ions to the shoulder is $\alpha \approx 0.02$ cm^{-1}, the maximum Fe^{2+} content can be calculated according to

$$\sigma = \alpha / c, \tag{1}$$

where c is the concentration of the corresponding impurity and α is the absorption coefficient. This results in $c_{Fe^{2+}} \leq 0.1$ wt. ppm. It means that, if Fe causes absorption, less than 10% of the entire Fe amount actually contributes to the absorption shoulder.

For e-wave light, analogous observations are made: comparing Fig. 1b to the peaks listed in Table 4 reveals that Fe^{2+} is most likely to cause the residual absorption around 21 350 cm^{-1} in the bottom part of the boule, but in this case the shoulder is less pronounced than for ordinarily polarized light. This is also expected, since the Fe shoulder around 21 510 cm^{-1} in e-wave spectra is weaker than the corresponding shoulder around 20 970 cm^{-1} in o-wave spectra [11].

4.1.3 Other transition metals

The GDMS data (Table 2) show that Ni and Cu are also present in the top part of the boule; however, these impurities cannot be detected in the bottom part of the boule within the measurement accuracy.

The o-wave absorption cross section of the Cu^{+} absorption peak at 20 970 cm^{-1} is $\sigma_{Cu^{+}} = 5.0 \times 10^{-18}$ cm^2 [15]. Assuming that $c_{Cu^{+}} \leq 0.1 c_{Cu}$, the absorption caused by Cu^{+} is smaller than 0.002 cm^{-1}.

Unfortunately, little is known about the absorption cross sections of Ni. However, taking the peak positions in Table 4 into account, the presence of Ni^{2+} might explain the small absorption peak at 23 400 cm^{-1} in o-wave spectra and, together with Cu^{+}, it may contribute to the o-wave-absorption shoulder in the entire spectral region between 25 000 and 18 200 cm^{-1}. In contrast, a significant contribution from Cu impurities can be excluded for e-wave spectra, since Cu does not show any significant absorption band between 20 000 and 25 000 cm^{-1} [14]. A small contribution from Ni cannot be excluded, because for Ni an absorption band is situated at 21 980 cm^{-1} for e-wave light.

4.2 Impurities in MgO-doped lithium niobate

Since the impurities most likely originate from the starting powders, one can expect to find similar impurities in MgO:LN as in CLN. Figure 3 shows this to be the case. Again, a pronounced absorption peak can be found at 15 200 cm^{-1} for o-wave light, as well as a second absorption band assumed to be composed of two absorption peaks with maxima at 19 000 and 20 350 cm^{-1}. This

double-peak structure is consistent with absorption spectra of Cr_2O_3:MgO:$LiNbO_3$ crystals with Mg-doping levels larger than 4.6 mol%, for which absorption peaks have been observed around 18 870 and 20 530 cm^{-1} [16]. Further support that Cr is causing the main absorption features is the weak, narrow peak at 13 750 cm^{-1}, which exactly coincides with the narrow absorption peak mentioned in [16]. As with CLN, it is possible that the underlying absorption shoulder is caused by Fe, Cu, and Ni.

4.3 Segregation of crystal impurities in congruent lithium niobate

The distribution coefficient of Cr in lithium niobate depends on many different parameters, such as the pulling and rotation rates during crystal growth and the electrical current flowing through the growing interface [17]. However, it is known that the distribution coefficient of Cr in $LiNbO_3$ is larger than unity, which agrees with our GDMS data. Hence, it is expected that Cr impurities in nominally undoped $LiNbO_3$ crystals show higher absorption in the top part of the boule than in the bottom part of the boule for almost the entire visible spectrum, as seen in Fig. 1. A Cr distribution coefficient larger than unity also means that the melt gets purer in Cr as more crystal material is grown out of it and solidified. This gives opportunities to get a purified melt concerning Cr and therefore get crystals that contain less Cr.

For MgO:LN, the distribution coefficient for Cr is also larger than unity [16] but, as mentioned before, MgO:LN boules are typically not grown using as large a melt fraction as for CLN boules and they are more complicated to grow. Therefore, purifying the melt through crystal growth might not be feasible.

Concerning crystal contamination of CLN with iron, there is no significant segregation of Fe in either the top or the bottom part of the boule. The GDMS data (Table 2) reveal an even distribution of Fe within the crystal.

4.4 Absorption cross sections in congruent lithium niobate

In order to be able to estimate the peak absorption amplitude from GDMS data instead of being forced to cut large pieces of crystals out of a boule to perform absorption spectroscopy, the absorption cross sections σ of the main contributing impurities have to be determined. The Fe^{2+} absorption cross sections in CLN are already known [11], but for Cr^{3+} there are several references giving different absorption cross sections, e.g. at 15 500 cm^{-1} the o-wave absorption cross sections found in the literature are 12×10^{-19} cm^2 [18], 8×10^{-19} cm^2 [19], and 0.14×10^{-19} cm^2 [20]. Thus, careful determination of the absorption cross sections for the respective Cr^{3+} absorption peaks from the data presented here is warranted.

Table 5 Chromium absorption cross sections in CLN. The values are determined with about 30% accuracy

Crystal	Peak (cm^{-1})	σ (cm^2)
CLN top: o-wave	15 300	6.5×10^{-19}
	20 850	1.9×10^{-19}
CLN bottom: o-wave	15 500	7.1×10^{-19}
	20 900	2.0×10^{-19}
CLN top: e-wave	15 550	2.2×10^{-19}
	21 350	1.5×10^{-19}
CLN bottom: e-wave	15 650	3.1×10^{-19}
	21 300	N/A

Using the amplitudes from the fits in Table 1 and the GDMS data from Table 2, the absorption cross sections of the top and the bottom CLN crystals are determined according to (1) and summarized in Table 5. For the o-wave absorption peak around 15 300 cm^{-1}, we see good consistency for the values determined for the two samples. Since the o-wave absorption at 20 850 cm^{-1} is not very pronounced and there is an underlying absorption shoulder, it is more reasonable to determine this particular absorption cross section in a different way: from Fig. 2, $\sigma_{20\,850,\mathrm{Cr}}$ can be estimated to be 3.5 times smaller than $\sigma_{15\,300,\mathrm{Cr}}$, yielding the values of the second row of Table 5. The weaker e-wave absorption peaks, at least in the top CLN cube, are clearly resolved against the underlying absorption shoulder, allowing a direct evaluation of the absorption cross section as for the o-wave spectra. The e-wave absorption cross section for the bottom CLN cube cannot be determined at 21 300 cm^{-1} because it is to small and because of the underlying absorption shoulder, as was discussed earlier. The results are summarized in Table 5.

Due to the fact that the accuracy of the GDMS data is about 30%, the accuracy of the absorption cross sections in Table 5 is about 30% as well. Additionally, for the bottom CLN cube the absorption peak fits are less precise, as was discussed earlier. The independently determined absorption cross sections at 15 300 cm^{-1} (o-wave) and 15 550 cm^{-1} (e-wave) agree with each other for the top and bottom CLN crystals within the accuracy limits. The o-wave absorption cross section for the peak centered at 15 300 cm^{-1} agrees with the one determined from [19]. The e-wave absorption cross section is not given in Refs. [19, 20] and the value in Table 5 does not agree with that provided in [18]. One explanation for the deviation of the Cr^{3+} absorption cross sections in Refs. [18, 20] from our values might be that the determination of the impurity content was less precise in these early studies.

4.5 Comparison: congruent lithium niobate versus MgO-doped lithium niobate

Unfortunately, we are not able to determine quantitatively the Cr^{3+} absorption cross section for MgO:LN, because the exact impurity concentrations of the MgO:LN samples are unknown; however, Fig. 3 and Table 3 clearly show that $\sigma_{\text{o-wave}}$ is up to one order of magnitude larger than $\sigma_{\text{e-wave}}$ around 19 000 cm^{-1} and about three times larger around 15 200 cm^{-1}. In contrast, in the CLN samples the absorption cross sections for e-wave and o-wave at a specified wavenumber do not differ by more than a factor of three (Table 5). Having low optical absorption for e-wave light is important in the design of high-power nonlinear-optical devices that operate in this spectral range, since mostly e-wave light is used in these applications due to the large nonlinear-optical coefficient.

As mentioned earlier, purification of the melt concerning Cr might be challenging but, fortunately, the e-wave Cr absorption cross section in MgO:LN is smaller than the corresponding o-wave Cr absorption cross section. This means that crystals with $\alpha < 0.015$ cm^{-1} are already attainable using e-wave light for wavenumbers smaller than 20 000 cm^{-1} due to the lower absorption cross section.

5 Conclusions

Absorption spectroscopy was performed with nominally undoped CLN and MgO:LN crystals as well as with Cr_2O_3-doped $LiNbO_3$. It turns out that Fe is not the only important contributor to optical absorption; in CLN the most pronounced absorption peaks, around 15 300 and 20 850 cm^{-1}, can be attributed to Cr^{3+} impurities at concentrations that are difficult to control, e.g. $c_{Cr} = 0.5$ wt. ppm for the crystal cut from the top part of the CLN boule.

Determination of the Cr^{3+} absorption cross sections confirms that the distribution coefficient of Cr is larger than unity, so that Cr is less incorporated into the bottom part of the boule than into the top part (by a factor of 10 for typical growth conditions). Thus, the absorption in the bottom part is decreased by up to a factor of 10 as well.

It was also seen that in these samples, typical of commercially grown LN, other transition metals, such as Cu, Mn, and Ni, caused minor absorption. For MgO:LN, chromium contributes significantly to the absorption as well, but fortunately absorption is lower than in CLN and is even lower for e-wave light, which is commonly used for nonlinear-optical applications. To further investigate the use of MgO:LN for high-power optical applications, studies are under way whose aim it is to decrease the impurity content of the problematic impurities in MgO:LN by a significant degree.

Acknowledgements J.R.S. gratefully acknowledges financial support of the Deutsche Telekom Stiftung. This research was supported in part by Crystal Technology, Inc., and AFOSR under grants FA9550-09-1-0233 and FA9550-05-1-0180.

References

1. D.A. Bryan, R. Gerson, H.E. Tomaschke, Appl. Phys. Lett. **44**, 847 (1984)
2. G.D. Miller, R.G. Batchko, W.M. Tulloch, D.R. Weise, M.M. Fejer, R.L. Byer, Opt. Lett. **22**, 1834 (1997)
3. S.T. Lin, Y. Lin, T.D. Wang, Y.C. Huang, Opt. Express **18**, 1323 (2010)
4. F. Jermann, K. Buse, Appl. Phys. B **59**, 437 (1994)
5. K. Buse, Appl. Phys. B **65**, 391 (1997)
6. D.H. Jundt, M.C.C. Kajiyama, D. Djukic, M. Falk, J. Cryst. Growth **312**, 1109 (2009)
7. L. Kovacs, G. Ruschhaupt, K. Polgar, G. Corradi, M. Wöhlecke, Appl. Phys. Lett. **70**, 2801 (1997)
8. D. Zelmon, D. Small, D. Jundt, J. Opt. Soc. Am. B **12**, 3319 (1997)
9. J. Workman Jr., *Applied Spectroscopy* (Academic Press, San Diego, 1998)
10. A.M. Glass, J. Chem. Phys. **50**, 1501 (1969)
11. H. Kurz, E. Krätzig, W. Keune, H. Engelmann, U. Gonser, B. Dischler, A. Räuber, Appl. Phys. **12**, 355 (1977)
12. M.G. Clark, F.J. DiSalvo, A.M. Glass, G.E. Peterson, J. Chem. Phys. **59**, 6209 (1973)
13. L. Arizmendi, J.M. Cabrera, F. Agullo-Lopez, Ferroelectrics **26**, 823 (1980)
14. J.R. Schwesyg, H.A. Eggert, K. Buse, E. Sliwinska, S. Khalil, M. Kaiser, K. Meerholz, Appl. Phys. B **89**, 15 (2007)
15. K. Peithmann, J. Hukriede, K. Buse, E. Krätzig, Phys. Rev. B **61**, 4615 (2000)
16. J. Diaz-Caro, J. Garcia-Sole, D. Bravo, J.A. Sanz-Garcia, F.J. Lopez, F. Jaque, Phys. Rev. B **54**, 13042 (1996)
17. A. Feisst, A. Räuber, J. Cryst. Growth **63**, 337 (1983)
18. D. Von der Linde, A.M. Glass, K.F. Rodgers, J. Appl. Phys. **47**, 217 (1976)
19. Y. Ming, E. Krätzig, R. Orlowski, Phys. Status Solidi A **92**, 221 (1985)
20. J.M. Almeida, G. Boyle, A.P. Leite, R.M. De La Rue, C.N. Ironside, F. Caccavale, P. Chakraborty, I. Mansour, J. Appl. Phys. **78**, 2193 (1995)